Fuel 381 (2025) 133603

Contents lists available at ScienceDirect

Fuel

journal homepage: www.elsevier.com/locate/fuel

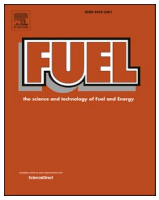

Full Length Article

# Interactive mechanisms of $CF_3CHFCF_3$ with $H_2$-$CH_4$-air mixture explosion: A synergistic study using chemical kinetic simulation and density functional theory

Hongfu Mi [a,b,*], Nan Luo [a], Peng Shao [c], Hang Yi [d,*], Shuo Wang [e], Wenhe Wang [a,b], Yihui Niu [a,b], Ao Yang [a,b], Xinsheng Jiang [f], Yu Feng [g], Li-Huan Zhu [h], Chi-Min Shu [h,*]

[a] College of Safety Engineering, Chongqing University of Science and Technology, Chongqing 401331, PR China
[b] Chongqing Key Laboratory for Oil and Gas Production Safety and Risk Control, Chongqing 401331, PR China
[c] College of Chemistry and Chemical Engineering, Southwest Petroleum University, Chengdu 610500, PR China
[d] Department of Mechanical and Materials Engineering, Wright State University, Dayton, OH 45435, USA
[e] School of Environmental Science and Safety Engineering, Tianjin University of Technology, Tianjin 300384, PR China
[f] Department of Oil, Army Logistical University, Chongqing 401331, PR China
[g] School of Chemical Engineering, Oklahoma State University, Stillwater, OK 74078, USA
[h] Department of Safety, Health, and Environmental Engineering, National Yunlin University of Science and Technology, 123, University Rd., Sec. 3, Douliou, Yunlin 64002, Taiwan, ROC

ARTICLE INFO

*Keywords:*
Thermal promotion mechanisms
Reaction pathway
Fluorine-containing radicals
Adiabatic flame temperature
Reactive radicals

ABSTRACT

To ascertain the underlying thermal promotion mechanism of $CF_3CHFCF_3$ in $H_2$-$CH_4$-air mixture fires, a comphensive investigation was conducted using chemical knetic simulation and density functional theory (DFT) calculation. The findings indicate that promotion or inhibition effects are determined by both time sequence and thermal characteristics of the main control reactions. As for lean-fuel conditions ($\Phi = 0.6$ and 0.8), $CF_3CHFCF_3$ decompose preferentially by 1,2-elimination reaction pathway generating $CF_3CH = CF_2$ rather than C–C bond cleavage reaction pathway when $CF_3CHFCF_3$ volume fraction is less than 4 %. The low-barrier addition reactions of $CF_3CH = CF_2$ double bond generate fluorine-containing radicals (e.g., $^{\bullet}CF_3$ and $^{\bullet}CF_2$). These fluorine-containing radicals release heat in the reaction with reactive radicals, thereby increasing the adiabatic flame temperature at lean-fuel flames. In the context of stoichiometric and rich-fuel ($\Phi \geq 1.0$) conditions, the rich reactant concentrations activate fluorine-containing radicals (e.g., $^{\bullet}CHFO$, $CHF_3$, and $^{\bullet}F$) to inhibiting explosion reactions by continueously depleting reactive radicals, absorbing the combustion temperature, and generating stable molecules. Additionally, the results also show that the generated $^{\bullet}C_3F_7$ presents exothermic properties, which is more apparently under lean-fuel conditions. Furthermore, it was observed that addition of $CF_3CHFCF_3$ can retard the explosive chain raction of $H_2$-$CH_4$-air mixture by competing $^{\bullet}H$ with $CH_4$. These findings provide theoretical guidance for the selection of halogenation suppressants to address the possible hydrogen-doped natural gas fires.

## 1. Introduction

A promising low-cost, possibly safer solution to introduce hydrogen (chemical formula: $H_2$) from end-production to end-users involves blending $H_2$ into the existing natural gas pipeline networks [1]. However, the accidental leak of such combustible and explosive mixtures could happen due to intrinsic characteristics (i.e., low ignition temperature, prompt burning rate, a wide range of explosion limits, etc.) of $H_2$, possibly leading to distinct consequences (i.e., fire and explosion accidents) in the production, storage, transport, and end-use [1–4]. The physical and chemical properties of $H_2$-blended gas mixtures are more complicated than those mixtures without $H_2$, particularly regarding dispersion and explosion [5]. Consequently, there is an urgent demand to develop an effective agent to suppress possibly triggered fires and explosions induced by $H_2$-$CH_4$-air mixtures [6].

Currently, halogenated extinguishing agents, especially Halon 1301 (chemical formula: $CF_3Br$) or Halon 1211 (chemical formula: $CF_2ClBr$),

* Corresponding authors.
*E-mail addresses:* mimihh5@163.com (H. Mi), hang.yi@wright.edu (H. Yi), shucm@yuntech.edu.tw (C.-M. Shu).

https://doi.org/10.1016/j.fuel.2024.133603
Received 6 June 2024; Received in revised form 6 October 2024; Accepted 30 October 2024

**Nomenclature**

| | |
|---|---|
| $A$ | Cross-sectional area of the stream plan encompassing the flame, [$cm^2$] |
| $c_p$ | Constant-pressure heat capacity, [J/K] |
| $c_{pk}$ | Constant-pressure heat capacity of the $k_{th}$ species, [J/K] |
| DFT | Density functional theory |
| $E_{elec}$ | Electronic energy, [J] |
| $E_{tot}$ | Partition function contribution, [–] |
| $G$ | Gibbs free energy, [kJ/mol] |
| ΔG | $G$ changes from $G_1$ to $G_2$, [kJ/mol] |
| $H$ | Enthalpy, [kJ/mol] |
| ΔH | $H$ changes from $H_1$ to $H_2$, [kJ/mol] |
| $h$ | Planck constant, [J·s] |
| $h_k$ | Specific enthalpy of the $k_{th}$ species |
| IRC | Intrinsic reaction coordinate |
| Im(v) | Imaginary part of the imaginary frequency, [1/cm] |
| $K$ | Total number of species, [–] |
| $k(T)$ | Reaction rate constant, [mol/($cm^3$ • s)] |
| $k_b$ | Boltzmann constant, [J/K] |
| $\dot{M}$ | Mass flow rate, [g/($cm^2$·s)] |
| 1-D | One dimensional |
| $P$ | Pressure, [atm] |
| $\dot{Q}_{rad}$ | Heat loss due to gas radiation, [J] |
| $R$ | Universal gas constant, [$m^3$·atm/(K·mol)] |
| $r$ | Pearson correlation coefficient |
| $S$ | Entropy, [J/(mol·K)] |
| ΔS | $S$ changes from $S_1$ to $S_2$, [J/(mol·K)] |
| $S_{vib}$ | Vibrational degree of freedom, [–] |
| $S_{rot}$ | Rotational degree of freedom, [–] |
| $S_{trans}$ | Translational degree of freedom, [–] |
| $T$ | Temperature, [K] |
| $V_k$ | Diffusion velocity of the $k_{th}$ species, [$cm^2$/s] |
| $W_k$ | Molecular weight of the $k_{th}$ species, [–] |
| $\overline{W}$ | Mean molecular weight, [–] |
| $X_{CF_3CHFCF_3}$ | Volumetric fraction of $CF_3CHFCF_3$, [%] |
| $X_{H_2}$ | Volumetric fraction of $H_2$, [%] |
| $x$ | Spatial coordinate, [–] |
| $Y_k$ | Mass fraction of the $k_{th}$ species, [–] |
| $ZPE$ | Zero-point correction energy, [kJ/mol] |

*Greek Letters*

| | |
|---|---|
| Φ | Equivalence ratio, [–] |
| $\rho$ | Mass density, [g/$cm^3$] |
| κ | Tunneling factor, [–] |
| $\lambda$ | Thermal conductivity, [J/(cm·K·s)] |
| $\dot{\omega}_k$ | Molar rate of the production by the chemical reaction of the $k_{th}$ species per unit volume, [mol/s] |
| $\sigma$ | Reaction path degeneracy, [–] |
| $\sigma_{TS}$ | Rotational symmetry number of the transition state structure, [–] |
| $\sigma_R$ | Rotational symmetry number of the reactants, [–] |

can effectively suppress gas-induced fires and/or explosions. But due to its unique chemical properties causing high ozone depletion potential, $CF_3Br$ and $CF_2ClBr$ have been banned and/or are restricted in use in various countries, such as China, Turkey, Singapore, India, with the Montreal Protocol agreement [7–10]. Alternatively, with great fire extinguishing effect and high diffusivity and thermostability, heptafluoropropane (chemical formula: $CF_3CHFCF_3$) could be a translationally ideal fire extinguishing agent that could replace some conventional suppressants, such as Halon 1301 [11,12]. However, recent investigations revealed that $CF_3CHFCF_3$ enhances the combustible ability of inflammable lean-fuel gas mixtures [13–16] (e.g., $CH_4$-air, $H_2$-$CH_4$-air, $H_2$-air, and $C_3H_8$-air) usually at low volumetric fraction and lean-fuel conditions. This phenomenon has attracted close attention in the fire protection and safety engineering research community to investigate the intrinsic mechanisms of such scenarios.

To investigate the underlying reaction mechanisms governing the explosive inhibition and promotion by $CF_3CHFCF_3$, researchers performed CHEMKIN simulation that the free radicals and the net heat

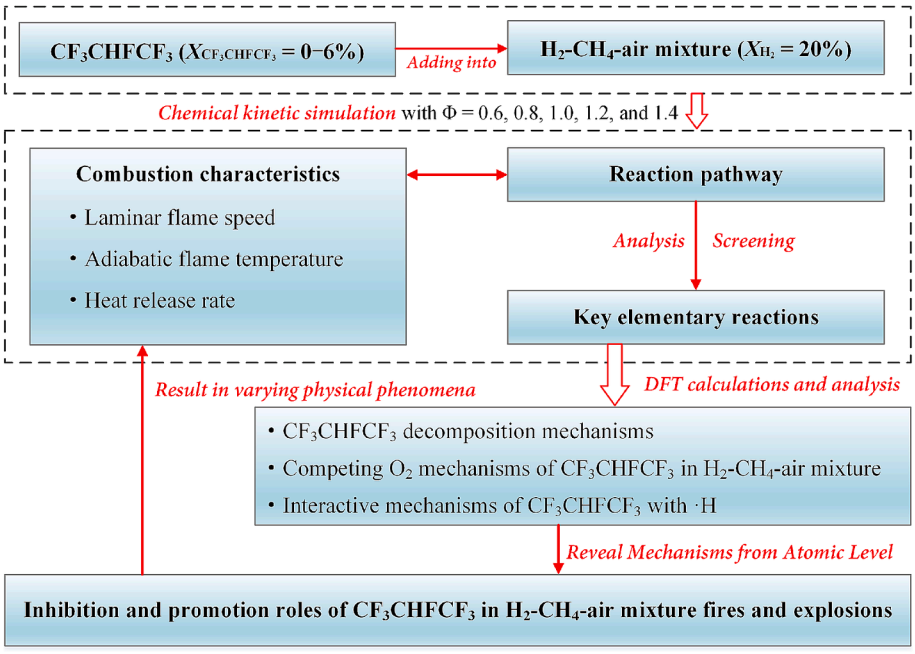


**Fig. 1.** The framework of this study.

release of lean-fuel explosion increased with low fraction $CF_3CHFCF_3$ addition, which resulted in an increase in temperature and promoted overall combustion [17–19]. Moreover, chemical kinetic simulation was employed to screen fluorine-containing reactions that facilitate combustion [20]. Notably, the $^{\bullet}CF_3$, $^{\bullet}CF_2$, and $^{\bullet}CFO$ reacting with $^{\bullet}H$ and $^{\bullet}OH$ contributed significantly to the heat release [21–23]. Nevertheless, the main reason why $CF_3CHFCF_3$ continues to be promoted exclusively under lean-fuel conditions with low fractions remains inadequately explained in existing studies. This is due to the limitations of CHEMKIN simulation with respect to predicting the time sequence and the exothermic quantities of reactions at the microscopic level. Therefore, in this study, a combination of chemical kinetic simulation and DFT calculation was employed to determine the promoting and inhibiting roles of $CF_3CHFCF_3$ within the $H_2$-$CH_4$-air mixture. Specifically, as the presented research pathway in Fig. 1, chemical kinetic simulation was first conducted to examine $CF_3CHFCF_3$ effects on the combustion characteristics (i.e., flame speed and adiabatic temperature) and identify main reaction pathways in the $H_2$-$CH_4$-air mixture. DFT was employed to establish the intrinsic kinetic properties and time sequence of key elementary reactions observed in reaction pathway analysis, offering insights into reaction mechanisms from molecular/atomic perspectives. The outcomes of the current work clarify $CF_3CHFCF_3$ performance (i.e., inhibition and promotion) in $H_2$-$CH_4$-air mixture fires/explosions from both pathways in chemical kinetic simulation and molecular analysis. This can assist fire suppression scientists and engineers in finding the prime $CF_3CHFCF_3$ formula to generate appropriate suppressants for such mixture fires/explosions.

## 2. Material and methods

### 2.1. Chemical kinetic simulation theory

The $H_2$-$CH_4$-air mixture explosion basically involves deflagration waves propagating from the burned to unburned mixtures; thus, a 1-D, planer, stationary, adiabatic premixed flame model was employed to simulate $H_2$-$CH_4$-air mixture combustion scenario. Specifically, the governing equations are given as Eqs. (1) to (4):

$$\dot{M} = \rho u A \tag{1}$$

$$\dot{M}\frac{dT}{dx} - \frac{1}{c_p}\frac{d}{dx}\left(\lambda A\frac{dT}{dx}\right) + \frac{A}{c_p}\sum_{k=1}^{K}\rho Y_k V_k c_{pk}\frac{dT}{dx} + \frac{A}{c_p}\sum_{k=1}^{K}\dot{\omega}_k h_k W_k + \frac{A}{c_p}\dot{Q}_{rad} = 0 \tag{2}$$

$$\dot{M}\frac{dY_k}{dx} + \frac{d}{x}(\rho A Y_k V_k) - A\dot{\omega}_k W_k = 0 \tag{3}$$

$$\rho = \frac{P\overline{W}}{RT} \tag{4}$$

where $\dot{M}$ is the mass flow rate; $\rho$ is mass density; $A$ is the cross-sectional area of the stream plan encompassing the flame; $T$ is temperature; $x$ represents the spatial coordinate; $c_p$ is the constant-pressure heat capacity of mixtures; $\lambda$ is the thermal conductivity of mixtures; $K$ is the total number of species; $Y_k$ is the mass fraction of the $k_{\text{th}}$ species; $V_k$ is diffusion velocity of the $k_{\text{th}}$ the species; $c_{pk}$ is the constant-pressure heat capacity of the $k_{\text{th}}$ species; $\dot{\omega}_k$ is the molar rate of the production by the chemical reaction of the $k_{\text{th}}$ species per unit volume; $h_k$ is specific enthalpy of the $k_{\text{th}}$ species; $W_k$ is the molecular weight of the $k_{\text{th}}$ species; $\dot{Q}_{rad}$ is heat loss due to gas radiation; $P$ is pressure; $\overline{W}$ is the mean molecular weight of the mixture; $R$ is the universal gas constant.

To determine the laminar flame speed under lean-fuel and rich-fuel conditions with various $X_{CF_3CHFCF_3}$(0–6 %) scenarios, five equivalence ratios Φ (i.e., Φ = 0.6, 0.8, 1.0, 1.2, and 1.4) were designated as initial conditions correspondingly, in which the volumetric fraction of $H_2$ ($X_{H_2}$) was designated as 20 % [4,24] in all designated Φ values of the $H_2$-$CH_4$-air mixture. It is worth mentioning that the selection of 20 % of $H_2$ blended into the mixture was due to such a ratio being commonly employed in many industrial applications with existing natural gas pipelines [25–28]. In addition, the mass flow rate was 0.04 g/(cm$^2$·s). Note that Φ is calculated based upon the mixtures without suppressant, illustrated as Eq. (5):

$$\Phi = \frac{(Fuel/Air)}{(Fuel/Air)_{\text{stitch}}} \tag{5}$$

where *Fuel/Air* is the volume ratio of the $H_2$-$CH_4$ mixture to air. The air was assumed to contain 21 % $O_2$ and 79 % $N_2$. All calculations were performed under initial conditions of 298 K and 1 atm.

The influence of the burning rate on laminar flame speed was investigated with designated inlet values of 0.01, 0.04, 0.08, 0.2, and 0.4 g/(cm$^2$·s). As shown in Fig. S1 in the Supplementary File, the mass flow rate has nearly no influence on the laminar flame speed under the same Φ. The curvature and gradient were decided as 0.016 by satisfying the relative difference smaller than 0.01 % in laminar flame speed between the employed computational mesh and finer mesh. The simulation tasks were performed using CHEMKIN-Pro 2022R1 (ANSYS, Canonsburg, PA, USA). The Soret effect [29] was considered in the calculation.

### 2.2. Chemical kenetic simulation validation

The reaction mechanisms of $H_2$-$CH_4$-air mixture flame with $CF_3CHFCF_3$ are based upon three distinct sub-mechanisms: AramcoMech 1.3 for removal of uncorrelated reactions, NIST C1-C3 HFC reactions, and $CF_3CHFCF_3$ decomposition and oxidation reactions. AramcoMech 1.3 (C3 version) was proposed by Metcalfe et al. [30] to characterise the kinetic and thermochemical properties of a large number of C1-C4 based hydrocarbon and oxygenated fuels under a wide range of experimental conditions, which was validated against a large number of experimental measurements with the specific data from shock tubes, flames, jet-stirred, plug-flow reactors, and rapid compression machines [31]. As described by its name, NIST C1-C3 HFC reactions were used to track the chemical kinetic reactions associated with HFC reactions in this study [32], and sub-mechanisms of $CF_3CHFCF_3$ reaction kinetics were developed by Williams et al. [33,34]. The entire reaction mechanisms for $CF_3CHFCF_3$ contain 183 species and 1302 elementary reactions in this study.

In this work, laminar flame speed is employed to validate chemical kinetic simulation model by comparing with previous publications [8,35–39] under various equivalence ratios and volumetric fractions of $CF_3CHFCF_3$. As shown in Fig. 2, the simulation results have good performance in matching previous data under varying equivalence ratios. Specifically, the flame speed in this study has a similar trend with the previous investigations along with the increased equivalence ratio. The predictions of laminar flame speed of $CH_4$-air mixture at 298 K and 1 atm are close to previous results [8,39] with registered $r$ = 0.9982, although the results in this study are slightly higher than the experimental values of Vagelopoulos et al. [35] under rich-fuel flames. Similarly, Fig. 3 depicts sound agreement in the results between chemical kinetic simulation and the data from Osorio et al. [20] and Zhang et al. [17] under varying volumetric fractions of $CF_3CHFCF_3$, with the registered $r$ = 0.9974 and 0.9995, respectively. Although some discrepancies still can be observed between chemical kinetic simulation and the previous work [40] under low volumetric fractions of $CF_3CHFCF_3$, because the experimental results [40] were obtained using a Mache-Hebra nozzle burner. Such a burner does not take into account the compression effects, heat loss, and stretching effects [41]. Therefore, based on the good agreement in laminar flame speed calculations between this study and previous experimental measurements, the chemical kinetic simulation model is qualified to investigate flame speed properties and secure key elementary reactions in $H_2$-$CH_4$-air mixture fires with $CF_3CHFCF_3$.

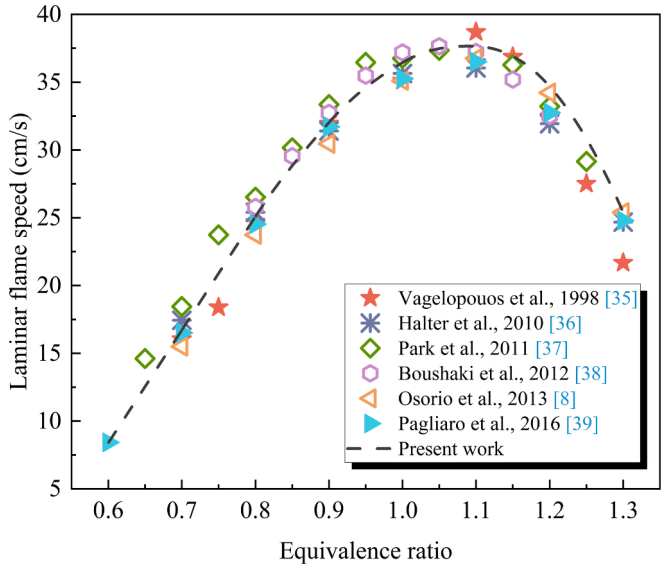


**Fig. 2.** The relationship of laminar flame speed and equivalent ratio in $CH_4$-air mixture fires at 298 K and 1 atm. Dotted symbols indicate published experimental results, and dashed line indicate calculated results.

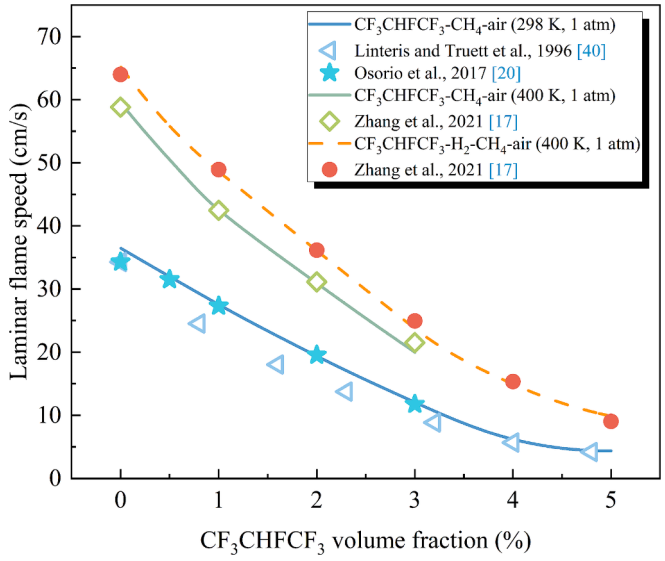


**Fig. 3.** The relationship of laminar flame speed and $CF_3CHFCF_3$ volume fraction in both $CH_4$-air and $H_2$-$CH_4$-air mixtures fires under various initial temperatures and pressures. Dotted symbols indicate published experimental results, solid line and dashed line indicate calculated results.

### 2.3. Density functional theory (DFT)

Through chemical kinetic simulation, key elementary reactions in the $CF_3CHFCF_3$-$H_2$-$CH_4$-air reaction system were assessed and selected to further investigate the reaction mechanism at the atomic level using DFT calculations. DFT has been widely employed in theoretical studies of organic molecules in terms of molecular dynamics [42–44]. In this study, the kinetic properties of key reactions were calculated using the Gaussian 16 W software package with B3LYP-D3 (BJ) functional [45] and D3(BJ) dispersion correction [46,47], along with the 6-31G(d) basis set for all atoms [48]. The geometrical configurations of all stationary points (i.e., reactants, products, and transition states) in the key elementary reactions were fully optimised at the B3LYP-D3(BJ)/6-31G (d), and a frequency analysis of the resulting stationary points was conducted to determine the zero-point corrected energy (*ZPE*) in the reaction system. This was compared with a previous study [49] showing the DFT-based B3LYP-D3(BJ) method can control the errors within 3 % in bond length calculations for H–H, C–H, H–F, O=O, C–F, O–H, and C=C, respectively, In this study, the theoretically calculated bond lengths and bond angles are in sound agreement with the experimental data [49] as well as the Perdew-Burke-Ernzerhof function calculated values [50,51] (see Figs. S2–S4 in Supplementary file). Thereafter, from the transition state, its correlations with reactants and products were confirmed using the intrinsic reaction coordinate (IRC) method [52]. Meanwhile, to gain more accurate single-point energies, the stationary point energies of optimised configurations were refined using CAM-B3LYP functional [53] with the basis sets of 6-311+G(d, p). To validate the reliability of CAM-B3LYP functional and 6-311+G(d, p) basis sets, the B3LYP-D3(BJ)/6-311+G(d, p), CAM-B3LYP/6-311+G(d, p), and M06-2X/6-311+G(d, p) methods were used to calculate the reaction paths of R2, R4, and R8. It is found that all the selected methods show the same trend of reaction paths and relative level of energy barriers (see Fig. S5 in the Supplementary File). Accordingly, the commonly used CAM-B3LYP/6-311+G(d, p) functional was employed for all calculations in this study. The calculated thermodynamic and kinetic data for the key elementary reactions can be accessed in the Supplementary file.

In the reaction system, enthalpy, *H*, entropy, *S*, and Gibbs free energy, *G*, were calculated using Eqs. (6)–(8):

$$H = E_{elec} + ZPE + E_{tot} \tag{6}$$

$$S = S_{vib} + S_{rot} + S_{trans} \tag{7}$$

$$G = H - TS \tag{8}$$

where $E_{elec}$ is electronic energy; *ZPE* is zero-point correction energy; $E_{tot}$ is partition function contribution; $S_{vib}$ is the vibrational degree of freedom; $S_{rot}$ is the rotational degree of freedom; $S_{trans}$ is the translational degree of freedom. Specifically, the change in G determines the chemical reaction direction when it proceeds at a constant temperature and pressure. For example, if G changes from $G_1$ to $G_2$, and $\Delta G = G_2\text{-}G_1 < 0$, the minimum energy to activate the reaction of state 1 is higher than state 2, indicating that the reaction can happen spontaneously. However, if $\Delta G = G_2\text{-}G_1 > 0$, the reaction cannot happen spontaneously. Therefore, based upon ΔG, the reaction direction under the constant temperature and pressure can be determined in the $CF_3CHFCF_3$ interaction with the $H_2$-$CH_4$-air mixture, which can be calculated by changes of enthalpy (ΔH) and entropy (ΔS), that is illustrated by Eq. (9):

$$\Delta G = \Delta H - T\Delta S \tag{9}$$

In this study, $E_a$ and $E_b$ are defined as the Gibbs free energy differences in transition state vs. reaction state and transition state vs. product state, respectively. Here, $E_a$ is considered the energy barrier for a reaction, and its magnitude shows the difficulty level specifically.

According to transition state theory [54], the reaction rate constants in the key elementary reaction channels can be calculated by Eqs. (10a) and (10b):

$$k(T) = k(T)\sigma\frac{k_b T}{h}\exp\left(-\frac{\Delta G}{RT}\right) \tag{10a}$$

$$\kappa = 1 + \frac{1}{24}\left[\frac{h\mathrm{Im}(v)}{k_b T}\right]^2 \tag{10b}$$

where $\sigma = \sigma_{TS}/\sigma_R$ is the reaction path degeneracy; $\sigma_{TS}$ is the rotational symmetry number of the transition state structure; $\sigma_R$ is the rotational symmetry number of the reactants; Boltzmann constant $k_b = 1.38064852 \times 10^{-23}$ J/K; Planck constant $h = 6.6260693 \times 10^{-34}$ J·s; $\kappa$ is the tunneling factor; Im(v) is the imaginary part of the imaginary frequency.

## 3. Results and discussion

### 3.1. Chemical kinetics in $CF_3CHFCF_3$-$H_2$-$CH_4$-air mixture deflagration

#### 3.1.1. Laminar flame speed and adiabatic flame temperature

The laminar flame speed and adiabatic flame temperature are two pivotal parameters in analysing $H_2$-$CH_4$-air combustion scenarios, serving as the key indicators of inhibiting performance [18,55,56]. As shown in Fig. 4, for all examined equivalence ratios in $H_2$-$CH_4$-air mixtures with initial conditions of 300 K and 1 atm, the addition of $CF_3CHFCF_3$ consistently led to a reduction in the laminar flame speed when $X_{CF3CHFCF3}$ increased from 0 to 6 %, aligning with previous experimental findings [13,15]. Specifically, when $X_{CF3CHFCF3} \leq 4$ %, the flame speed was determined by equivalence ratio. Under $\Phi = 0.6$, the laminar flame speed was 7.2 cm/s when $X_{CF3CHFCF3} = 4$ %, and the decreasing rate was roughly 46.2 % compared with the flame without $CF_3CHFCF_3$. At the same $CF_3CHFCF_3$ volume fraction, the decreasing percentage was approximately 68.5 %, 84.1 %, 88.3 %, and 80.9 % for $\Phi = 0.8$, 1.0, 1.2, and 1.4, respectively. The laminar flame speeds of different equivalence ratios were close when $X_{CF3CHFCF3} > 4$ %. The result suggests that the inhibition and promotion effects of $CF_3CHFCF_3$ are not affected by the equivalence ratio when the volume fraction is higher. In addition, the history slope of laminar flame speed is markedly increased as the hydrogen-methane mixture approaches the stoichiometric ratio ($\Phi = 1.0$). This phenomenon is attributed to the fact that when the $H_2$-$CH_4$ concentration nears the stoichiometric ratio, it becomes easier for the reactants and oxygen to undergo complete reaction. Meanwhile, there is a more pronounced dilution effect of $CF_3CHFCF_3$ on oxygen and consumption of $^{\bullet}CH_3$ [13], leading to an accelerated decrease in the rate of laminar flame speed.

As can be seen from Fig. 5, at the lean-fuel conditions considered ($\Phi = 0.6$ and 0.8, 300 K and 1 atm), the addition of $CF_3CHFCF_3$ exhibits an adverse effect that the exothermic reaction of the molecule with oxygen and the fuel augments the heat release and raises the adiabatic flame temperature. Note that compared with the continuous reduction of laminar flame speed for each equivalence ratio mixture, the adiabatic flame temperature increases as more $CF_3CHFCF_3$ is added when $X_{CF3CHFCF3} \leq 4$%. Specifically, the adiabatic flame temperature increased to 2349 and 2407 K, with $X_{CF3CHFCF3} = 4$% for $\Phi = 0.6$ and 0.8, respectively. The addition of $CF_3CHFCF_3$ enhanced the heat release from the combustion of the $H_2$-$CH_4$-air mixture, which ultimately led to

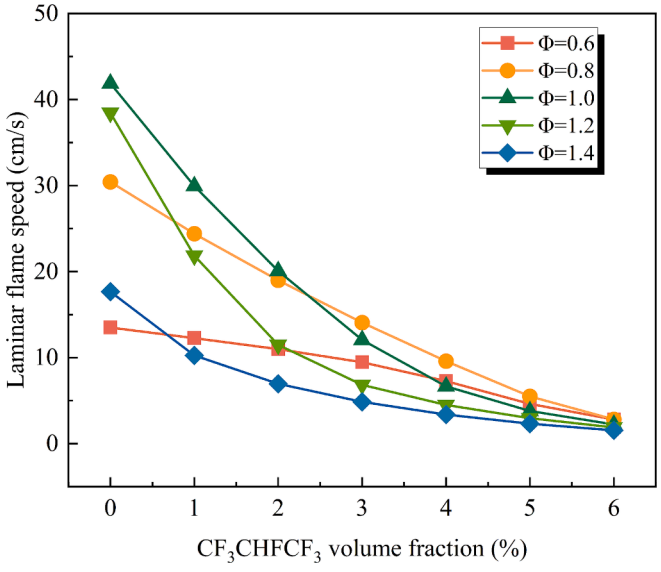


**Fig. 4.** Laminar flame speed of $H_2$-$CH_4$-air mixture with different $CF_3CHFCF_3$ volume fractions.

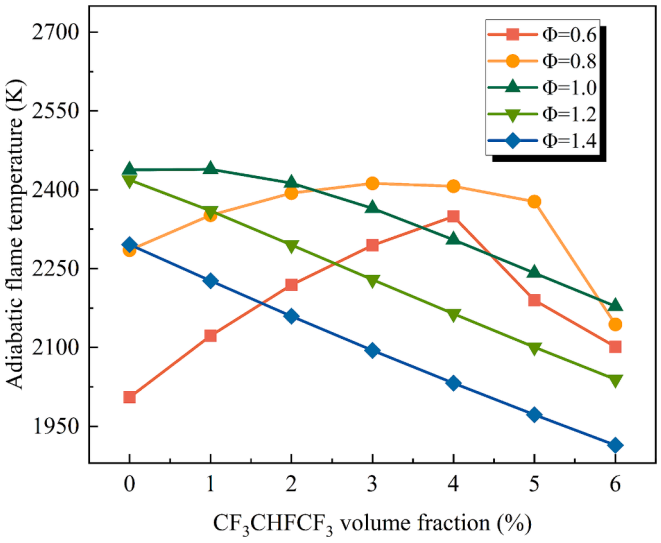


**Fig. 5.** Adiabatic flame temperature of $H_2$-$CH_4$-air mixture with different $CF_3CHFCF_3$ volume fractions.

an increase in the adiabatic flame temperature [17,57]. Simultaneously, the elevated combustion temperature promoted the combustion process by accelerating the reaction rate of chain branching reactions and the concentration of reactive radicals [18]. As the volume fraction of $CF_3CHFCF_3$ increased, fluoride played dominant role in the trapping of key radicals, such as $^{\bullet}H$, $^{\bullet}OH$, and $^{\bullet}HO_2$, thus inhibiting the reaction from proceeding. Under rich-fuel and stoichiometric conditions ($\Phi \geq 1$), the adiabatic flame temperature and $X_{CF_3CHFCF_3}$ presented a linear relationship, and more $CF_3CHFCF_3$ led to a decrease in flame temperature gradually.

#### 3.1.2. Key heat-releasing elementary reactions

The heat release rate, an inherent characteristic of combustible mixtures, reflects both the chemical reaction rate and the heat release from the flames. Hence, to determine the effect of $CF_3CHFCF_3$ addition on the thermal effect of the $H_2$-$CH_4$-air mixture combustion system and to reveal the elementary reactions affecting the adiabatic flame temperature of the combustion system, the heat release rate of the $H_2$-$CH_4$-air mixture at 300 K and 1 atm, $X_{CF3CHFCF3} = 4$ % and three designated equivalence ratios, i.e., $\Phi = 0.6$, 1.0, and 1.2, were considered. The heat release rate in Fig. 6 indicates that the primary fluorinated reactions that contribute to the positive heat release rate are $^{\bullet}CF_3 + {}^{\bullet}H = {}^{\bullet}CF_2 + HF$, $^{\bullet}CH_3 + {}^{\bullet}CF_3 = CH_2{:}CF_2 + HF$, and $CF_3CHF^{\bullet} + {}^{\bullet}OH = CF_3CHO + HF$; these are exothermic reactions, although they can reduce radical concentrations. When these exothermic reactions become predominant in lean-fuel flames with lower $CF_3CHFCF_3$ additions ($X_{CF3CHFCF3} \leq 4$ %), additional heat is produced. Such a phenomenon can be also explained by the adiabatic flame temperature increasing gradually when $X_{CF3CHFCF3}$ changes from 0 to 4 % (see Fig. 5). Among various fluorinated-reactions and all designated equivalence ratios, the thermal decomposition process of $CF_3CHFCF_3$ (i.e., $C_3F_7H(+M) = {}^{\bullet}CF_3 + CF_3CHF^{\bullet}$ (+M)) consumes the greatest energy among all elementary reactions (see Fig. 6). It is noteworthy that at $\Phi = 1.2$, the fluoride-containing exothermic reactions $CF_3CHF^{\bullet} + {}^{\bullet}OH = CF_3CHO + HF$, $^{\bullet}CF_2 + {}^{\bullet}OH = {}^{\bullet}CFO + HF$, $^{\bullet}CF_3 + {}^{\bullet}OH = CF_2O + HF$, $CF_3CHF^{\bullet} + {}^{\bullet}O = {}^{\bullet}CF_3 + CHFO$, and $^{\bullet}CF + {}^{\bullet}OH = CO + HF$ disappeared and the new additional reactions $^{\bullet}H + {}^{\bullet}CH_3(+M) = CH_4(+M)$, $HCCO + O_2 = {}^{\bullet}H + CO + CO_2$ released heat, but not as much as the heat release rate from small fluoride-containing molecules trapping reactive radicals at $\Phi = 0.6$. This is mainly due to the reduced reaction rates of the major exothermic reactions $^{\bullet}CF_3 + {}^{\bullet}H <=> {}^{\bullet}CF_2 + HF$, $CF_3CHF^{\bullet} + {}^{\bullet}OH <=> CF_3CHO + HF$, and $^{\bullet}CH_3 + {}^{\bullet}CF_3 <=> CH_2{:}CF_2 + HF$, as shown in Figs. S6 (a–c) in the

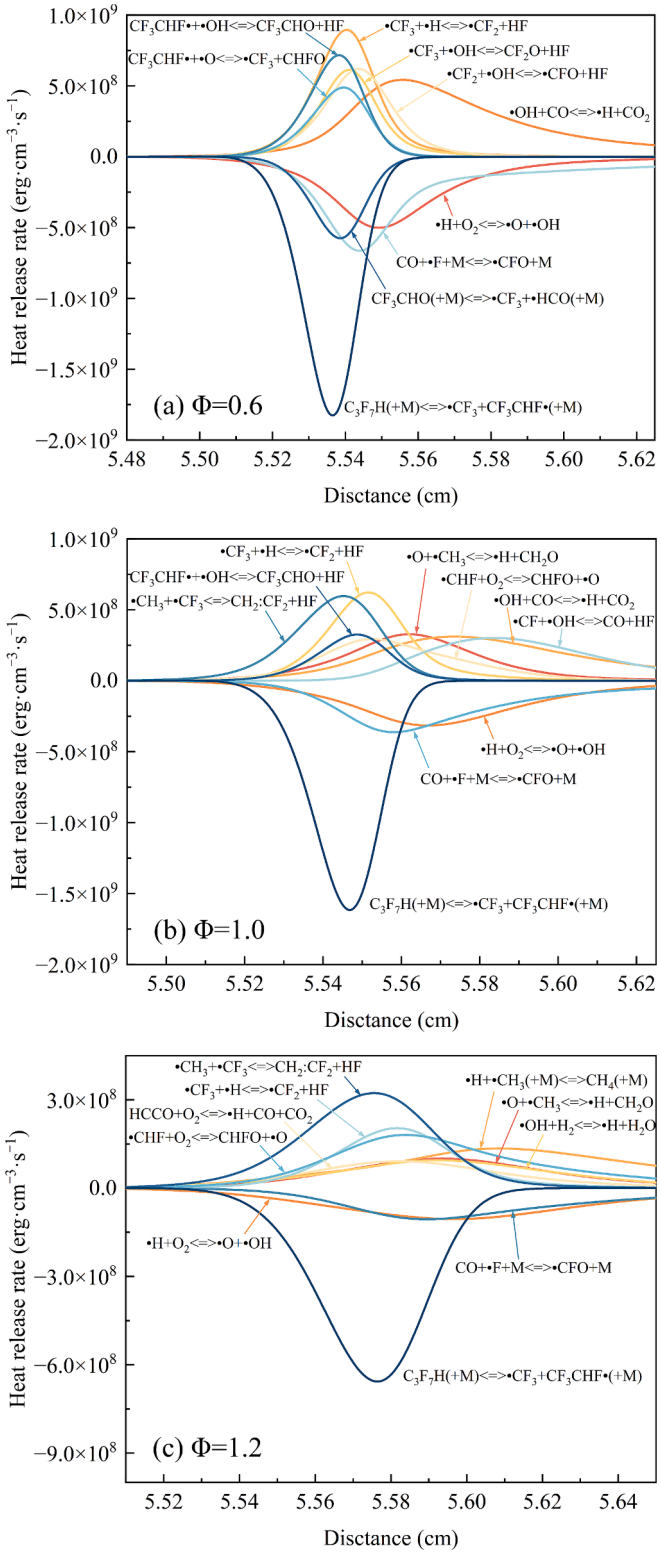


**Fig. 6.** The contributions of the main elementary reactions to heat release of $H_2$-$CH_4$-air mixture flames with Φ = 0.6, 1.0, and 1.2, $X_{H_2}$= 20 %, but$X_{CF_3CHFCF_3}$ = 4 %.

Supplementary File. As illustrated in Fig. 7, the global heat release rate decreased with increasing equivalence ratio, and the peak of the global heat release rate moved downstream. This suggests that the the onset of the exothermic reactions were delayed as the concentration of the reacting substrate increased. This finding is in accordance with the

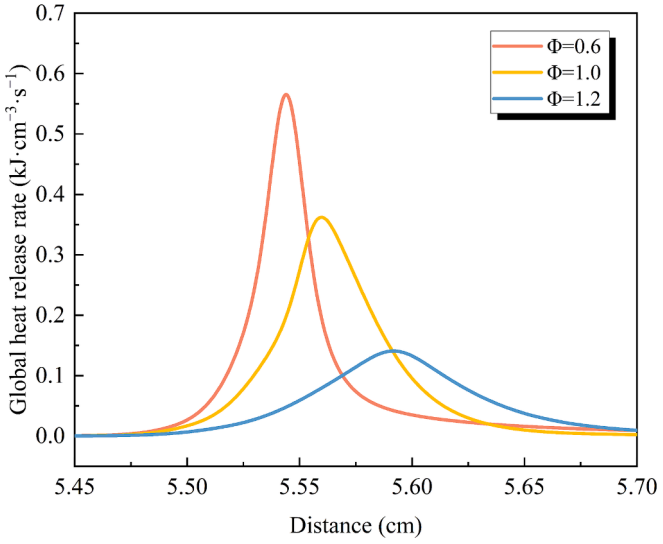


**Fig. 7.** Global heat release rate of $H_2$-$CH_4$-air mixture flames with Φ = 0.6, 1.0, and 1.2, $X_{H_2}$= 20 %, but$X_{CF_3CHFCF_3}$ = 4 %.

observed trend in the heat release rate profile as a function of the equivalence ratio. Overall, the chemical inhibitory effect of the $CF_3CHFCF_3$ addition gradually led to a decrease in the concentration of reactive radicals in the combustion system with an increase in reactants, and the fluoride-containing exothermic reaction was gradually replaced, resulting in a remarkable decrease in the overall heat release rate.

### 3.1.3. *$CF_3CHFCF_3$ reaction pathways*

To secure the main elementary reactions of $CF_3CHFCF_3$ in the lean-fuel flame, which influenced $H_2$-$CH_4$-air mixture deflagration, the reaction pathways of $CF_3CHFCF_3$ at$X_{CF_3CHFCF_3}$ = 4 % in $H_2$-$CH_4$-air mixture systems at Φ = 0.6 were investigated based upon the substance consumption rates in the combustion process, as illustrated in Fig. 8. The primary reaction pathway of $CF_3CHFCF_3$ → HF in the explosion process is the C–C bond cleavage reaction pathway: $CF_3CHFCF_3$ → $CF_3CHF^{\bullet}$ → $^{\bullet}CF_3$ → HF, accounting for 59.2 % of the $CF_3CHFCF_3$. As the second largest $CF_3CHFCF_3$ consumer, the 1,2-HF elimination reaction pathway $CF_3CHFCF_3$ → $CF_3CF{=}CF_2$ → $CF_3CHF^{\bullet}$ → $^{\bullet}CHFO$ → HF is also an important route, encompassing 25 % correspondingly. During the process of $CF_3CHFCF_3$ decomposition, a large amount of $^{\bullet}CF_3$ was generated, ~25 % of which generated HF and $CH_2 = CF_2$ molecules with $^{\bullet}CH_3$ in the following reactions. Such reactions can effectively delay the development of the $CH_4$ → $CO_2$ reaction pathway. As depicted in Fig. 8, the final product of fluoride-containing substances was HF. This reflected the fire-extinguishing characteristics of $CF_3CHFCF_3$, and the F atom was like a "disposable" fire-extinguishing medium. If sufficient $^{\bullet}H$ exists in the reaction system, no matter which reaction pathway is taken, the final product, i.e., HF molecules, can be generated continuously.

## 3.2. *Key elementary reactions*

To investigate the main factors influencing the reaction path changes during the initial stage of the combustion system, nine elementary reactions were selected based upon the results of the reaction pathway analysis (see Table 1). The reaction rate constants, $k(T)$, for each elementary reaction were obtained by numerical calculations, as listed in Table 2.

### 3.2.1. *$CF_3CHFCF_3$ decomposition mechanisms*

As seen in Table 1, the most important elementary reactions of the $CF_3CHFCF_3$ decomposition process in $H_2$-$CH_4$-air mixtures mainly consist of reaction (1) (R1) and reaction (2) (R2), i.e., 1,2-HF elimination

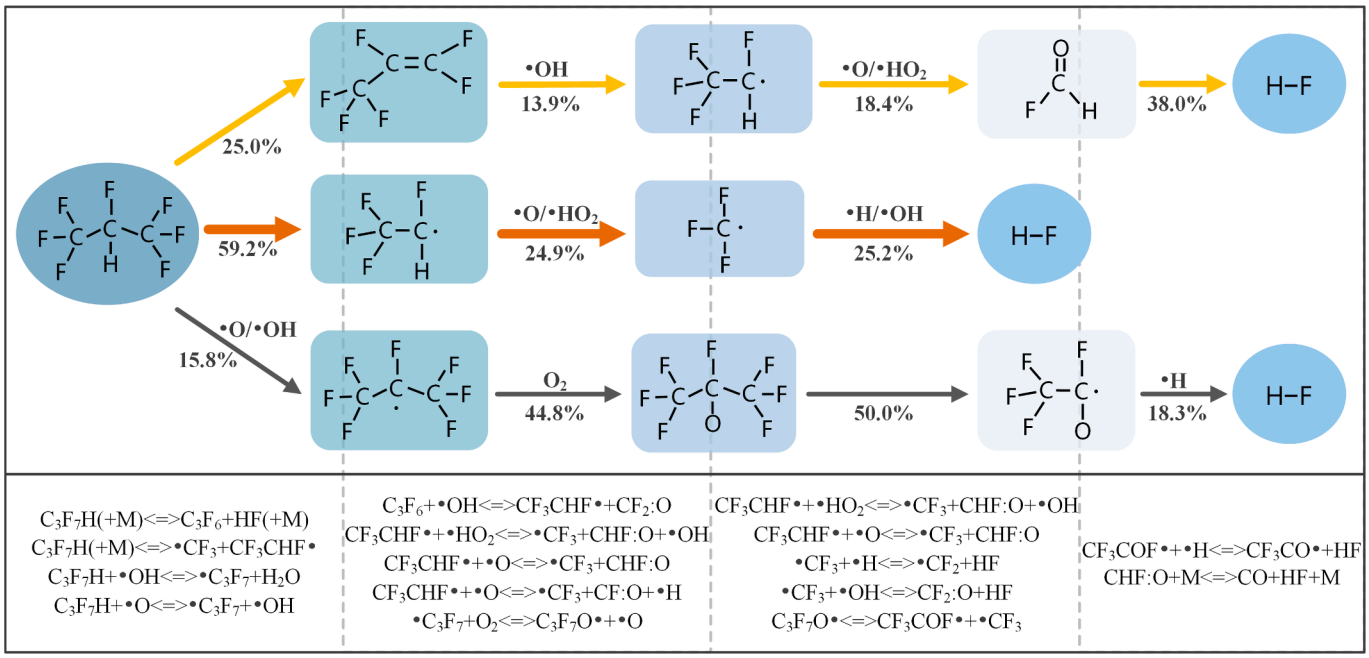


**Fig. 8.** Decomposition pathways of $CF_3CHFCF_3$ to HF at $\Phi = 0.6$, with$X_{H_2} = 20$ % and$X_{CF_3CHFCF_3} = 4$ %.

**Table 1**
Key elementary reactions affecting the initial stage.

| No. | Reaction | Thermodynamic property | | Kinetic property |
|---|---|---|---|---|
| Reaction (1) | $C_3F_7H$ => $C_3F_6$ + HF | Heat absorption | Non-spontaneous reaction | $E_a > E_b$ facilitates progress |
| Reaction (2) | $C_3F_7H$ => $^{\bullet}CF_3$ + $CF_3CHF^{\bullet}$ | Heat absorption | Non-spontaneous reaction | – |
| Reaction (3) | $^{\bullet}C_3F_7 + O_2$ <=> $C_3F_7O_2^{\bullet}$ | Heat release | Spontaneous reaction | – |
| Reaction (4) | $^{\bullet}C_3F_7 + O_2$ <=> $C_3F_7O$ + $^{\bullet}O$ | Heat release | Spontaneous reaction | $E_a < E_b$ facilitates progress |
| Reaction (5) | $H_2 + O_2$ <=> $^{\bullet}HO_2 + {}^{\bullet}H$ | Heat absorption | Non-spontaneous reaction | $E_a > E_b$ facilitates progress |
| Reaction (6) | $CH_4 + O_2$ <=> $^{\bullet}CH_3 + {}^{\bullet}HO_2$ | Heat absorption | Non-spontaneous reaction | $E_a > E_b$ facilitates progress |
| Reaction (7) | $CH_2O + O_2$ <=> $^{\bullet}HO_2 + {}^{\bullet}HCO$ | Heat absorption | Non-spontaneous reaction | $E_a > E_b$ facilitates progress |
| Reaction (8) | $C_3F_7H + {}^{\bullet}H$ <=> $^{\bullet}C_3F_7 + H_2$ | Heat release | Spontaneous reaction | $E_a < E_b$ facilitates progress |
| Reaction (9) | $CH_4 + {}^{\bullet}H$ <=> $^{\bullet}CH_3 + H_2$ | Heat absorption | Spontaneous reaction | $E_a < E_b$ facilitates progress |

**Table 2**
Thermodynamic and dynamic data and reaction rate constants of key elementary reactions.

| | Reaction rate (mol/cm$^3$ • s$^{-1}$) | $\Delta H$(kJ/mol) | $\Delta G$(kJ/mol) | $E_a$(kJ/mol) | $E_b$(kJ/mol) |
|---|---|---|---|---|---|
| 1 | $4.62\times10^{-61}$ | 178.70 | 119.11 | 306.76 | 187.66 |
| 2 | $1.40\times10^{-66}$ | 376.09 | 338.26 | – | – |
| 3 | $9.93\times10^{-21}$ | −108.85 | −76.55 | – | – |
| 4 | $8.85\times10^{-50}$ | −116.26 | −77.40 | 242.37 | 319.76 |
| 5 | $4.64\times10^{-54}$ | 197.32 | 195.63 | 266.80 | 71.17 |
| 6 | $5.60\times10^{-47}$ | 223.51 | 240.27 | 240.36 | 2.10 |
| 7 | $3.47\times10^{-49}$ | 151.51 | 147.69 | 238.98 | 91.29 |
| 8 | $2.24\times10^{-14}$ | −15.73 | −3.01 | 48.25 | 51.26 |
| 9 | $3.02\times10^{-16}$ | 2.45 | −0.45 | 50.96 | 51.41 |

and C–C bond cleavage reaction (see Fig. 8). In R1, the H3 atom to be eliminated was rarely activated, which can be seen from the evidence that its bond length only increased by 0.33293 Å (see Fig. 9). It implies that the F atom on the edge carbon of $CF_3CHFCF_3$ would be activated first, leading to C–F bond break. F6 atom moved away from the C4 atom, and the bond length R(C4, F6) increased from 1.33556 to 1.89182 Å. Then, substantial loosening of the H3 atoms occurred after the reaction reached the transition state (TS1). Owing to the unique electron-withdrawing ability of the F6 atom [58], the neighbouring H3 atom detached from the reaction system along with F6 atom elimination until a stable HF molecule and $CF_3CF{=}CF_2$ with carbon–carbon double bonds

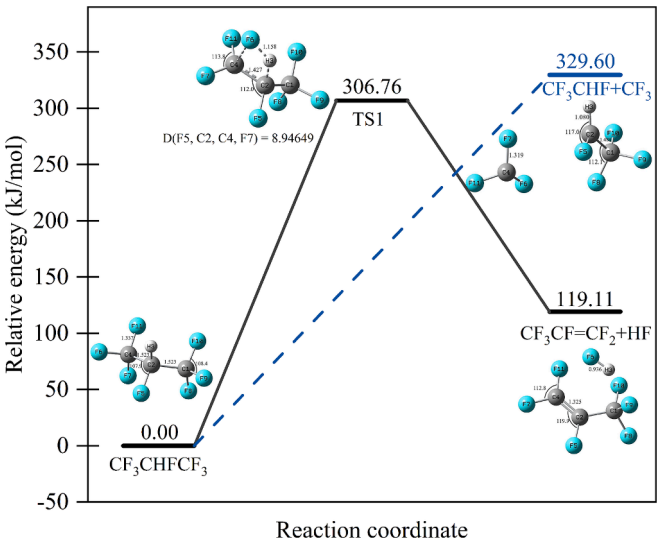


**Fig. 9.** Energy diagram of $CF_3CHFCF_3$ decomposition.

were formed after TS1. In the R1 channel, Gibbs free energy became 119.1 kJ/mol, and it absorbed heat of 178.7 kJ/mol. In R2, the C–C single bond break led to the formation of $CF_3CHF^{\bullet}$ and $^{\bullet}CF_3$, which is a simple bond-breaking reaction without a transition state. In addition, the bond length of R (C2,C4) increased from 1.52342 to 3.47360 Å, and the product dihedral angle D (F5,C2,F6,C4) of 58.08649° was deflected by nearly 180°. R2 was also an endothermic reaction, 376.1 kJ/mol; its Gibbs free energy turned out to be 329.6 kJ/mol. It indicates that under standard temperature and pressure conditions, R1 and R2 cannot happen spontaneously.

In addition, it needed more energy (i.e., $\Delta G_{R2} - Ea_{R1} = 31.5$ kJ/mol) to activate C–C bond cleavage reaction than 1,2-HF elimination reaction. The same results can be found by comparing the reaction rate constants (see Table 2), indicating that 1, 2-HF elimination reaction can happen easier than C–C bond cleavage reaction under same conditions. It suggests that at the initial stage of the $H_2$-$CH_4$-air mixture reaction system, $CF_3CHFCF_3$ can produce HF to dilute the reactant concentration and decrease the collision probability between the reactants and radicals.

### 3.2.2. *Competing $O_2$ mechanisms of $CF_3CHFCF_3$ in $H_2$-$CH_4$-air mixture*

To investigate the inhibiting performance of $CF_3CHFCF_3$ in the $H_2$-$CH_4$-air mixture reaction system ($\Phi = 0.6$), it was necessary to determine the mechanisms of how it contested oxygen with $H_2$ and $CH_4$. As depicted in Table 1, Reaction (5) (R5) and Reaction (6) (R6) were the initial stage reactions in the hydrogen-methane oxidation process, and Reaction (3) (R3) and Reaction (4) (R4) also are required to consume oxygen. As shown in Fig. 10, R3 had no transition state in which O–O, a single bond, was not stable and then formed an inactive radical, i.e., $C_3F_7O_2^{\bullet}$ with $^{\bullet}C_3F_7$. It was an exothermic reaction with 108.9 kJ/mol, and Gibbs free energy became −76.6 kJ/mol. In R4, the O=O double bond breaks, forming two oxygen atoms before it connected with C2 and F6 in TS2 in the same plane. Here, $^{\bullet}C_3F_7$ was unstable and would accept a free oxygen atom O11. In this process, R (C2, O11) decreased gradually from 1.65242 to 1.32530 Å, where the bonding condition was satisfied, resulting in the formation of $C_3F_7O$ and $^{\bullet}O$ Gibbs free energy became 123.4 kJ/mol and the exothermic heat was 116.3 kJ/mol.

Similarly, in R5 and R6, oxygen experienced double bond breakage and then formed an unstable O-O single bond induced by free radicals. Meanwhile, the H atom in the stabilised $H_2$ and $CH_4$ was attacked by free radicals and then entered transition states, i.e., TS3 and TS4, respectively. As shown in Fig. 11, the C1-H3 bond can be activated by the interaction with O7, and R (C1,H3) extended from 1.09180 to 1.93012 Å, resulting in the formation of $^{\bullet}CH_3$ and $^{\bullet}H$. This process has to overcome a free energy barrier of 242.4 kJ/mol and then absorbed heat of 223.5 kJ/mol. From Fig. 12, H1 in $H_2$ can be activated by O4 in $O_2$, and R (H1,O4) decreased from 3.24871 to 0.95346 Å to satisfy the bonding condition, finally forming $^{\bullet}HO_2$ and $^{\bullet}H$. The process needs to overcome the free energy barrier of 266.8kJ/mol and absorb heat of 197.3kJ/mol, specifically. In addition, at standard temperature and pressure, R3 and R4 can spontaneously happen, while R5 and R6 need extra heat/higher pressure/or related catalysts to activate the reaction based upon $\Delta G$ changes in the corresponding reactions (see Table 2). It suggests that the addition of $CF_3CHFCF_3$ to the $H_2$-$CH_4$-air mixture could effectively consume oxygen and generate inactive free radical $C_3F_7O_2^{\bullet}$ and $C_3F_7O^{\bullet}$, resulting in reducing reactive radical concentrations and oxygen, which are essential substances in the reaction with $CH_4$ and $H_2$. However, note that the reaction of the $^{\bullet}C_3F_7$ with $O_2$ releases heat. As can be seen from Fig. 8, 15.8 % of the $CF_3CHFCF_3$ molecules decompose into $^{\bullet}C_3F_7$, and then 44.8 % of the $^{\bullet}C_3F_7$ react exothermically, and the heat released from this process has a non-negligible influence on the global heat release.

A key chain branching reaction in the $CH_4$ explosion (see Reaction (7) (R7) in Table 1 and Fig. 13) [59], $H_2$ near oxygen in formaldehyde was activated first, and R(C1, H2) gradually increased from 1.09110 to 1.39557 Å. Then, $H_2$ gradually approached O5, forming TS5 in Fig. 13). R (H2, O5) gradually decreased from 1.17109 to 1.00232 Å to form $^{\bullet}HO_2$

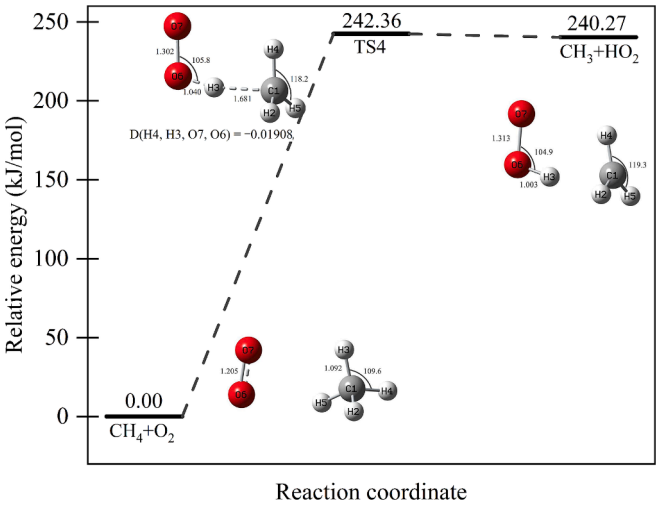


**Fig. 11.** Energy diagram for the reaction of $CH_4$ with $O_2$.

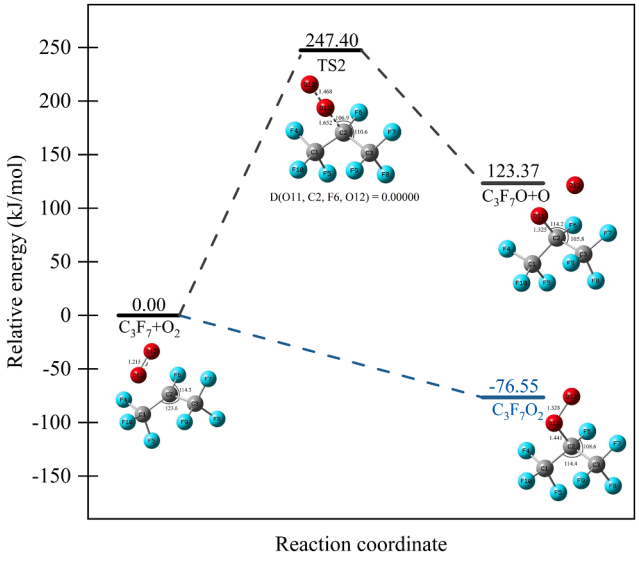


**Fig. 10.** Energy diagram for the reaction of $^{\bullet}C_3F_7$ with $O_2$.

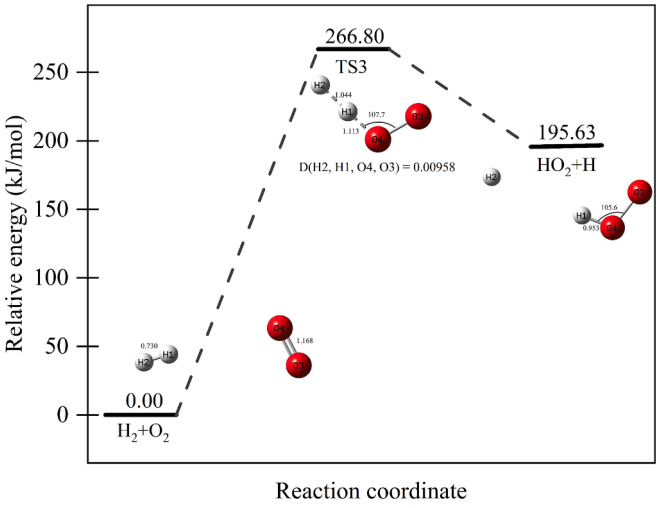


**Fig. 12.** Energy diagram for the reaction of $H_2$ with $O_2$.

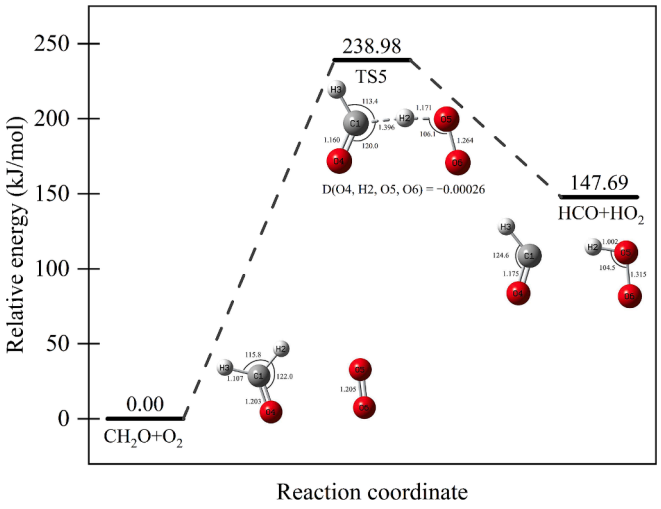


**Fig. 13.** Energy diagram for the reaction of $CH_2O$ with $O_2$.

and ˙HCO. The process required to overcome a free energy barrier of 239.0 kJ/mol and absorb heat of 151.5 kJ/mol. Note that R7 cannot spontaneously proceed under standard temperature and pressure due to $\Delta G > 0$. Nevertheless, it can be discovered that $E_a = 239.0$ kJ/mol and $k(T) = 9.93 \times 10^{-21}$ mol/(cm$^3$·s) in R7 are substantially higher than the values in R3, respectively (see Table 2), revealing that R3 is more likely to happen than R7. The decomposition product $^{\cdot}C_3F_7$ can prefer to react with $O_2$ in the branching chain of the entire $H_2$-$CH_4$-air mixture explosion system. Previous studies also support such findings that the fire-inhibiting properties of $CF_3CHFCF_3$ in the initial stage since its pyrolysis process would continuously consume heat and lower temperature in the combustion system [7,60].

### 3.2.3. *Interactive mechanisms of $CF_3CHFCF_3$ with ˙H*

How to alleviate ˙H in the $H_2$-$CH_4$-air mixture combustion system by reacting with $CF_3CHFCF_3$ can notably affect its suppression performance [17]; thus, it is essential to investigate the interactive mechanisms between $CF_3CHFCF_3$ and ˙H. Previous investigation showed that ˙H concentration would be increased notably after adding hydrogen into the mixture, and the generation rate was much faster than the generation rate of ˙OH [61], leading to not enough ˙OH to consume the extra ˙H promptly. In the initial reaction stage, i.e., Reaction (8) (R8), the ˙H on $CF_3CHFCF_3$ will be activated first, and the C–H bond breaks. R(C2, H3) increase from 1.09422 to 1.35869 Å to form TS6 (see Fig. 14). At TS6, H3 gradually moves towards ˙H to form $H_2$, and the other active radical (i.e., $^{\cdot}C_3F_7$) will be generated. In this process, $\Delta G = -3.0$ kJ/mol and releasing heat of 15.7 kJ/mol. The similar reaction mechanisms can be found in Reaction (9) (R9), in which ˙H attacks H4 to form TS7 (see Fig. 15), and R (C1,H4) increases from 1.09239 to 2.74705 Å. H5 interacts with H6 to produce $^{\cdot}CH_3$ and $H_2$, with $\Delta G = -0.5$ kJ/mol and absorption heat of 2.4 kJ/mol. Here, it can be found that R8 and R9 can happen spontaneously with $\Delta G < 0$ under standard temperature and pressure conditions, by overcoming the energy barriers of 48.2 and 51.0 kJ/mol, respectively. Moreover, R8 is more likely to happen than R9, with a greater reaction rate under the same reacting conditions. In this process, $CF_3CHFCF_3$ can capture ˙H quickly and efficiently, reducing the reaction rate of $CH_4$ and ˙H to form $^{\cdot}CH_3$. In addition, $^{\cdot}C_3F_7$ generated by R8 can also rapidly transfer to the next reaction stage, contesting $O_2$ with other reactive reactants and radicals. Therefore, $CF_3CHFCF_3$ plays an effective role in the initial stage of the $H_2$-$CH_4$-air mixture reaction chain.

### 3.3. *Dual roles of $CF_3CHFCF_3$: Promotion and inhibition*

Fig. 16 illustrates the interactive mechanisms between $CF_3CHFCF_3$ and $H_2$-$CH_4$-air mixture under$X_{CF_3CHFCF_3} \leq 4$ % and various Φ values, using reaction pathway analysis and DFT calculations. Fig. 16(a) demonstrates the reaction mechanism by which $CF_3CHFCF_3$ contributes to the thermal promotion of lean $H_2$-$CH_4$-air mixture explosions. Specifically, because the energy barrier of 1,2-HF elimination reaction is lower than that of C–C cleavage reaction, partial $CF_3CHFCF_3$ will first decompose into $CF_3CF = CF_2$ at the initial reaction stage. The rest of $CF_3CHFCF_3$ will be decomposed via C–C bond cleavage reaction and free radical-induced decomposition, forming $^{\cdot}CF_3$, $CHF_3CHF^{\cdot}$, $(CF_3)_2CF^{\cdot}$, $^{\cdot}CF_3CHO$, etc. Although $CF_3CF = CF_2$ accounts for a relatively small proportion in the pool of fluorinated radicals, it is a critical intermediate in the decomposition process. Specifically, with the double bond, $CF_3CF{=}CF_2$ will have additive reactions promptly with ˙H, ˙O, and ˙OH since the energy barriers are extremely low, which has been discussed in previous investigations [62,63], resulting in the generation of an immense number of fluoride-containing radicals (e.g., $^{\cdot}CF_2$, and $^{\cdot}CF_3$). Note that most reactions between small and fluorinated molecules were exothermic, which also has been proven by a previous investigation [18] as well as discussed in Section 3.1.2. As a result, the total heat release rate will increase during this phase, and the heat in the combustion system will increase as well, generating a thermal promotion phenomenon. Especially under lean-fuel conditions, the concentration of reactive radicals is relatively low, and the small, fluorinated molecules

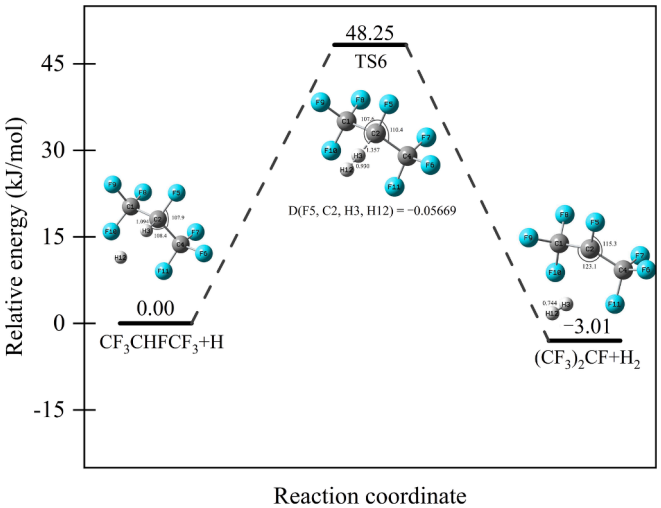


**Fig. 14.** Energy diagram for the reaction of $CF_3CHFCF_3$ with ˙H.

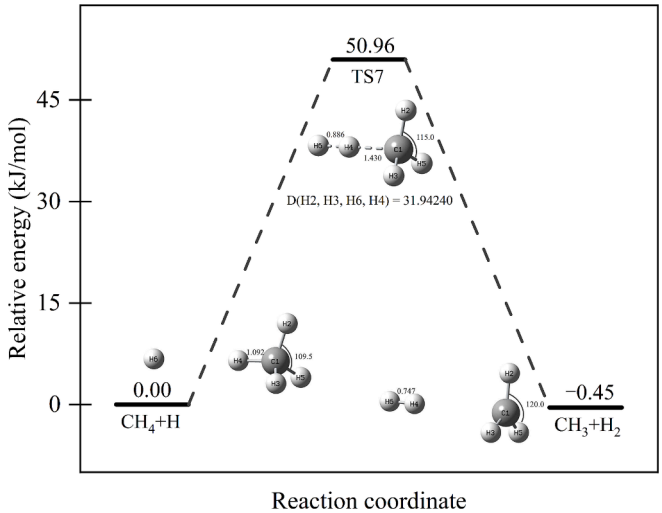


**Fig. 15.** Energy diagram for the reaction of $CH_4$ with ˙H.

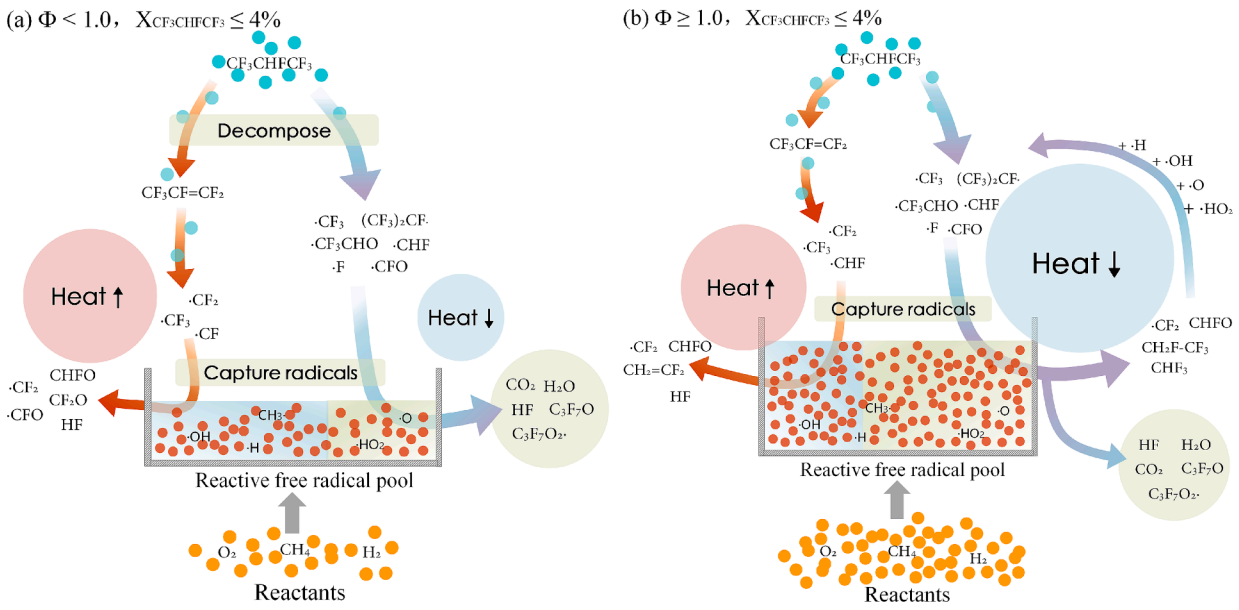


**Fig. 16.** Mechanism analysis diagram affecting the explosion: (a) $\Phi < 1.0$ and$X_{CF_3CHFCF_3} \leq 4$ % and (b) $\Phi \geq 1.0$ and$X_{CF_3CHFCF_3} \leq 4$ %.

generated by $CF_3CF = CF_2$ first capture the reactive radicals to react and then release heat (see Fig. 16(a)). In addition, the reactions associated with C–C bond cleavages and free radical-induced generation of small, fluorinated molecules will also consume reactive radicals, absorbing heat from the combustion system. However, under lean-fuel conditions (i.e., $\Phi < 1$) and low $X_{CF_3CHFCF_3}$, the absorbed heat is less than the released heat in the entire reaction system. It means that although the reactive radicals will be consumed in the combustion system, the total heat release rate will increase, presenting the $CF_3CHFCF_3$ promotion property with$X_{CF_3CHFCF_3} \leq 4$ %. In contrast, under $\Phi \geq 1$ condition (see Fig. 16(b)), the reactive radical concentrations can remain relatively high, and the heat-absorbing fluoride-related reaction will continue to consume the reactive radicals and absorb heat, presenting the $CF_3CHFCF_3$ inhibition property. Moreover, the reaction generates an increasing number of stabilised molecules and stabilised radicals, which reduces the effective collision of the reactants and thus impedes the mixture detonation.

## 4. Conclusions

To reveal the main reasons for the thermal promotion of $CF_3CHFCF_3$ within lean $H_2$-$CH_4$-air mixture explosion with various $X_{CF_3CHFCF_3}$ and designate Φ, this study employed chemical kinetic simulation and DFT calculations from theoretical and molecular perspectives to determine the promoting and inhibiting roles of $CF_3CHFCF_3$ within $H_2$-$CH_4$-air mixture. The key conclusions are listed below:

- The addition of $CF_3CHFCF_3$ into the $H_2$-$CH_4$-air mixture fire can decrease laminar flame speed in various Φ, and more $CF_3CHFCF_3$ can perform better in flame speed reduction. In addition, the mass flow rate nearly had no influence on the laminar flame speed under the same Φ. Under $\Phi \geq 1$ condition; adding more $CF_3CHFCF_3$ into the $H_2$-$CH_4$-air mixture lowers the adiabatic flame temperature. In comparison, under $\Phi < 1$ condition, the adiabatic flame temperature increases to a threshold and then decreases gradually, as $CF_3CHFCF_3$ is added into mixtures continuously.
- In lean-fuel flames, the C–C bond cleavage and 1,2-HF elimination are two main reaction pathways in the process of $CF_3CHFCF_3$ decomposition, with the latter being more favoured. During the initial stage, the $^{\cdot}H$ initially interacts with $CF_3CHFCF_3$, forming the secondary product $^{\cdot}C_3F_7$, a potent competitor for $O_2$ alongside $CH_4$ and $H_2$. It is worth noting that the heat generated by the reaction of the $^{\cdot}C_3F_7$ with $O_2$ has a non-negligible effect on the global heat release.
- $CF_3CF{=}CF_2$ is a vital intermediate in the process of $CF_3CHFCF_3$ decomposition, which can be rapidly broken down by radical addition reactions, contributing to an increase in the exothermic fluoride-containing radicals. Interactions between these radicals generated by $CF_3CF{=}CF_2$ addition reactions and reactive radicals are predominantly exothermic, resulting in an acceleration of heat release rate and promotion of flame propagation under certain conditions, such as $X_{CF_3CHFCF_3} \leq 4$ % and $\Phi = 0.6$. As the concentration of reactants increases (i.e., $\Phi > 1.0$), the non-exothermic fluorine-containing radicals are capable of mitigating the effects caused by thermal promotion through cyclically consuming reactive radicals and absorbing heat, thereby suppressing the hydrogen-methane-air mixture detonation.

## CRediT authorship contribution statement

**Hongfu Mi:** Writing – original draft, Methodology, Conceptualization. **Nan Luo:** Writing – original draft, Investigation, Formal analysis. **Peng Shao:** Writing – original draft, Investigation, Formal analysis. **Hang Yi:** Writing – review & editing, Resources. **Shuo Wang:** Writing – review & editing. **Wenhe Wang:** Methodology, Conceptualization. **Yihui Niu:** Methodology, Conceptualization. **Ao Yang:** Methodology, Conceptualization. **Xinsheng Jiang:** Methodology, Conceptualization. **Yu Feng:** Writing – review & editing, Resources. **Li-Huan Zhu:** Writing – review & editing. **Chi-Min Shu:** Writing – review & editing, Resources, Conceptualization.

## Declaration of competing interest

The authors declare that they have no known competing financial interests or personal relationships that could have appeared to influence the work reported in this paper.

## Acknowledgements

This work was financially supported by the National Natural Science Foundation of China (NSFC 5227-4177, 5170-4054), the Natural Science Foundation of Chongqing Scientific and Technological

(CSTB2023NSCQ-MSX0862), and Chongqing Institute of Science and Technology Master's Degree Innovation Program Project (YKJCX2220706). The authors are indebted to OSU Computational Biofluidics and Biomechanics Laboratory for the computational resources. This research was sponsored by the use of ANSYS codes as part of the ANSYS-WSU academic partnership agreement and is gratefully acknowledged the help received from Ms. Christine Taylor, Mr. Mark Mohrmann, and Mr. Vishaal Ganore.

## Appendix A. Supplementary data

Supplementary data to this article can be found online at https://doi.org/10.1016/j.fuel.2024.133603.

## Data availability

Data will be made available on request.

## References

[1] Chen YY, Long LW, Niu J, Huang TM, Chen X, Zhang J, et al. Investigation on the combustion characteristics and environmental effects of hydrogen-doped natural gas for domestic water heaters. ACS Omega 2023;8:48370–80. https://doi.org/10.1021/acsomega.3c07418.
[2] Van den Schoor F, Hermanns RTE, Oijen JA, Verplaetsen F, de Goey LPH. Comparison and evaluation of methods for the determination of flammability limits, applied to methane/hydrogen/air mixtures. J Hazard Mater 2008;150(3):573–81. https://doi.org/10.1016/j.jhazmat.2007.05.006.
[3] Li P, Huang P, Liu ZY, Du BX, Li MZ. Experimental study on vented explosion overpressure of methane/air mixtures in manhole. J Hazard Mater 2019;374:349–55. https://doi.org/10.1016/j.jhazmat.2019.04.046.
[4] Shirvill LC, Roberts TA, Royle M, Willoughby DB, Sathiah P. Experimental study of hydrogen explosion in repeated pipe congestion-Part 2: Effects of increase in hydrogen concentration in hydrogen-methane-air mixture. Int J Hydrogen Energy 2019;44(5):3264–76. https://doi.org/10.1016/j.ijhydene.2018.12.021.
[5] Cristello JB, Yang JM, Hugo R, Lee YS, Park SS. Feasibility analysis of blending hydrogen into natural gas networks. Int J Hydrogen Energy 2023;48(46):17605–29. https://doi.org/10.1016/j.ijhydene.2023.01.156.
[6] Wang B, Rao ZM, Xie QF, Wolanski P, Rarata G. Brief review on passive and active methods for explosion and detonation suppression in tubes and galleries. J Loss Prev Process Ind 2017;49:280–90. https://doi.org/10.1016/j.jlp.2017.07.008.
[7] Babushok V, Noto T, Burgess DRF, Hamins A, Tsang W. Influence of $CF_3I$, $CF_3Br$, and $CF_3H$ on the high-temperature combustion of methane. Combust Flame 1996;107(4):351–67. https://doi.org/10.1016/S0010-2180(96)00052-1.
[8] Osorio CH, Vissotski AJ, Petersen EL, Mannan MS. Effect of $CF_3Br$ on $C_1$–$C_3$ ignition and laminar flame speed: Numerical and experimental evaluation. Combust Flame 2013;160(6):1044–59. https://doi.org/10.1016/j.combustflame.2013.01.025.
[9] Pagliaro JL, Linteris GT, Sunderland PB, Baker PT. Combustion inhibition and enhancement of premixed methane-air flames by halon replacements. Combust Flame 2015;162(1):41–9. https://doi.org/10.1016/j.combustflame.2014.07.006.
[10] Secretariat UNEPO. Montreal protocol on substances that deplete the ozone layer as either adjusted and/or amended in London 1990, Copenhagen 1992, Vienna 1995, Montreal 1997, and Beijing 1999 (2000).
[11] Li GC, Wang XS, Xu HL, Liu YP, Zhang HP. Experimental study on explosion characteristics of ethanol gasoline-air mixture and its mitigation using heptafluoropropane. J Hazard Mater 2019;378:120711. https://doi.org/10.1016/j.jhazmat.2019.05.104.
[12] Robin ML. Climate change and the HFC-based clean extinguishing agents. Int Fire Protec 2012:20–4.
[13] Cao XY, Lu YW, Jiang JC, Wang ZR, Wei HY, Li YM, et al. Experimental study on explosion inhibition by heptafluoropropane and its synergy with inert gas. J Loss Prev Process Ind 2021;71:104440. https://doi.org/10.1016/j.jlp.2021.104440.
[14] Hamins A, Borthwick P. Suppression of ignition over a heated metal surface. Combust Flame 1998;112:161–70. https://doi.org/10.1016/S0010-2180(97)81764-6.
[15] Dong ZQ, Liu LJ, Chu YY, Su ZK, Cai C, Chen XF, et al. Explosion suppression range and the minimum amount for complete suppression on methane-air explosion by heptafluoropropane. Fuel 2022;328:125331. https://doi.org/10.1016/j.fuel.2022.125331.
[16] Yang K, Chen SJ, Ji H, Xing ZX, Hao YM, Zheng K, et al. Experimental study on the coupling effect of heptafluoropropane and obstacles with different slits on the methane-air explosion. Energy 2023;269:125331. https://doi.org/10.1016/j.energy.2023.126798.
[17] Zhang X, Yang Z, Huang X, Wang XY, Pan YL, Zhou XM. Combustion enhancement and inhibition of hydrogen-doped methane flame by HFC-227ea. Int J Hydrogen Energy 2021;46(41):21704–14. https://doi.org/10.1016/j.ijhydene.2021.03.250.
[18] Fan RJ, Wang ZR, Guo WJ, Lu YW. Experimental and theoretical study on the suppression effect of $CF_3CHFCF_3$ (FM-200) on hydrogen-air explosion. Int J Hydrogen Energy 2022;47(26):13191–8. https://doi.org/10.1016/j.ijhydene.2022.02.062.
[19] Mi HF, Shao P, Luo N, Wang S, Wang Y, Jiang XS, et al. Determination of $CF_3CHFCF_3$ suppression effects on premixed hydrogen-methane deflagration via experiment and simulation. Fuel 2023;358:130190. https://doi.org/10.1016/j.fuel.2023.130190.
[20] Osorio C, Morones A, Hargis JW, Petersen EL, Mannan MS. Effect of $C_2HF_5$ and $C_3HF_7$ on methane and propane ignition and laminar flame speed: Experimental and numerical evaluation. J Loss Prev Process Ind 2017;48:21–31. https://doi.org/10.1016/j.jlp.2017.04.003.
[21] Wang T, Sheng YH, Liang H, Yu YY, Cheng FM, Li RK, et al. Reducing the unwanted deflagration enhancement of $C_3HF_7$ on fuel-lean hydrogen-air mixture by diluting $CO_2$: An experimental and numerical research. Int J Hydrogen Energy 2024;57(6):812–21. https://doi.org/10.1016/j.ijhydene.2024.01.073.
[22] Wang T, Sheng YH, Liang H, Yu YY, Cheng FM, Li RK, et al. Experimental investigation and numerical analysis on the confined deflagration behavior of methane-air mixtures within the suppression of typical haloalkanes. Process Saf Environ 2024;183:87–98. https://doi.org/10.1016/j.psep.2024.01.002.
[23] Babushok VI, Linteris GT, Meier OC. Combustion properties of halogenated fire suppressants. Combust Flame 2012;159(12):3569–75. https://doi.org/10.1016/j.combustflame.2012.07.005.
[24] Erdener BC, Sergi B, Guerra OJ, Chueca AL, Pambour K, Brancucci C, et al. A review of technical and regulatory limits for hydrogen blending in natural gas pipelines. Int J Hydrogen Energy 2023;48(14):5595–617. https://doi.org/10.1016/j.ijhydene.2022.10.254.
[25] Wen X, Wang M, Su T, Zhang S, Pan R, Ji W. Suppression effects of ultrafine water mist on hydrogen/methane mixture explosion in an obstructed chamber. Int J Hydrogen Energy 2019;44(60):32332–42. https://doi.org/10.1016/j.ijhydene.2019.10.110.
[26] Duan Y, Long F, Huang J, Jia H, Bu Y, Yu S. Effects of porous materials with different thickness and obstacle layout on methane/hydrogen mixture explosion with low hydrogen ratio. Int J Hydrogen Energy 2022;47(63):27237–49. https://doi.org/10.1016/j.ijhydene.2022.06.065.
[27] Isaac T. Hy Deploy: The UK's first hydrogen blending deployment project. Clean Energy 2019;3(2):114–25. https://doi.org/10.1093/ce/zkz006.
[28] Wang S, Xiao GQ, Mi HF, Feng Y, Chen J. Experimental and numerical study on flame fusion behavior of premixed hydrogen/methane explosion with two-channel obstacles. Fuel 2023;333(2):126530. https://doi.org/10.1016/j.fuel.2022.126530.
[29] García-Ybarra P, Nicoli C, Clavin P. Soret and dilution effects on premixed flames. Combust Sci Technol 1984;42(1–2):87–109. https://doi.org/10.1080/00102208408960370.
[30] Metcalfe WK, Burke SM, Ahmed SS, Curran HJ. A hierarchical and comparative kinetic modeling study of C1–C2 hydrocarbon and oxygenated fuels. Int J Chem Kinet 2013;45(10):638–75. https://doi.org/10.1002/kin.20802.
[31] Ji CW, Wang D, Yang JX, Wang SF. A comprehensive study of light hydrocarbon mechanisms performance in predicting methane/hydrogen/air laminar burning velocities. Int J Hydrogen Energy 2017;42(27):17260–74. https://doi.org/10.1016/j.ijhydene.2017.05.203.
[32] Babushok VI, Donald R, Burgess DR, Kim DK, Hegetschweiler MJ, Linteris GT. Modeling of combustion of fluorine containing refrigerants. NIST 2021. https://doi.org/10.6028/NIST.TN.2170.
[33] Williams BA, L'Espérance DM, Fleming JW. Intermediate species profiles in low-pressure methane/oxygen flames inhibited by 2-H heptafluoropropane: Comparison of experimental data with kinetic modeling. Combust Flame 2000;120(1–2):160–72. https://doi.org/10.1016/S0010-2180(99)00081-4.
[34] Hynes RG, Mackie JC, Masri AR. Inhibition of premixed hydrogen-air flames by 2-H heptafluoropropane. Combust Flame 1998;113(4):554–65. https://doi.org/10.1016/S0010-2180(97)00267-8.
[35] Vagelopoulos CM, Egolfopoulos FN. Direct experimental determination of laminar flame speeds. 20th International symposium on combustion 1998;27(1):513–519. https://doi.org/10.1016/S0082-0784(98)80441-4.
[36] Halter H, Tahtouh T, Mounaïm-Rousselle C. Nonlinear effects of stretch on the flame front propagation. Combust Flame 2010;157(10):1825–32. https://doi.org/10.1016/j.combustflame.2010.05.013.
[37] Park O, Veloo PS, Liu N, Egolfopoulos FN. Combustion characteristics of alternative gaseous fuels. P Combust Inst 2011;33(1):887–94. https://doi.org/10.1016/j.proci.2010.06.116.
[38] Boushaki T, Dhué Y, Selle L, Ferret B, Poinsot T. Effects of hydrogen and steam addition on laminar burning velocity of methane–air premixed flame: Experimental and numerical analysis. Int J Hydrogen Energy 2012;37(11):9412–22. https://doi.org/10.1016/j.ijhydene.2012.03.037.
[39] Pagliaro PJ, Bouvet N, Linteris GT. Premixed flame inhibition by $CF_3Br$ and $C_3H_2F_3Br$ (2-BTP). Combust Inst 2016;169:272–86. https://doi.org/10.1016/j.combustflame.2016.04.017.
[40] Linteris GT, Truett L. Inhibition of premixed methane-air flames by fluoromethanes. Combust Flame 1996;105(1–2):15–27. https://doi.org/10.1016/0010-2180(95)00152-2.
[41] Strehlow RA, Savage LD. The concept of flame stretch. Combust Flame 1978;31:209–11. https://doi.org/10.1016/0010-2180(78)90130-X.
[42] Becke AD. Density-functional thermochemistry. III. The role of exact exchange. J Chem Phys 1993;98(7):5648–52. https://doi.org/10.1063/1.464913.
[43] Effeti II, Majoumo-Mbe F, Louis H, Nfor EN, Akongwi M, Unimuke TO, et al. Modeling of photofunctional transition metals (Mn, Re, Ir) complexes towards the effective detection of uric acid (UA) as biomarker for kidney dysfunction. J Photochem Photobiol A 2023;444:114942. https://doi.org/10.1016/j.jphotochem.2023.114942.
[44] Zhang LL, Li TJ, Zhang YD, Dong YN, Zhou LY, Zhou Q, et al. Simulation and experimental study on mechanism and kinetics of 1,1,2-trichloroethane

dehydrochlorination reaction. Chem Eng Sci 2022;262:117990. https://doi.org/10.1016/j.ces.2022.117990.
[45] Grimme S, Antony J, Ehrlich S, Krieg H. A consistent and accurate ab initio parametrization of density functional dispersion correction (DFT-D) for the 94 elements H-Pu. J Chem Phys 2010;132(15):154104. https://doi.org/10.1063/1.3382344.
[46] Parr RG, Gadre SR, Bartolotti LJ. Local density functional theory of atoms and molecules. P Natl Acad Sci USA 1979;76(6):2522–6. https://doi.org/10.1073/pnas.76.6.2522.
[47] Smith DGA, Burns LA, Patkowski K, Sherrill CD. Revised damping parameters for the D3 dispersion correction to density functional theory. J Phys Chem Lett 2016;7(12):2197–203. https://doi.org/10.1021/acs.jpclett.6b00780.
[48] Nielsen IMB, Seidl ET, Janssen CL. Accurate structures and binding energies for small water clusters: The water trimer. J Chem Phys 1999;110:845–59. https://doi.org/10.1063/1.478908.
[49] Kaye GWC, Laby TH. Tables of physical and chemical constants, 16th ed. Tables of physical & chemical constants 1995, Essex, England: Longman.
[50] Xu X, Goddard WA. The extended Perdew-Burke-Ernzerhof functional with improved accuracy for thermodynamic and electronic properties of molecular systems. J Chem Phys 2004;121(9):4068–82. https://doi.org/10.1063/1.1771632.
[51] Paier J, Hirschl R, Marsman M, Kresse G. The Perdew-Burke-Ernzerhof exchange-correlation functional applied to the G2–1 test set using a plane-wave basis set. J Chem Phys 2005;122(23):234102. https://doi.org/10.1063/1.1926272.
[52] Maeda S, Harabuchi Y, Ono Y, Taketsugu T, Morokuma K. Intrinsic reaction coordinate: Calculation, bifurcation, and automated search. Int J Quantum Chem 2015;115(5):258–69. https://doi.org/10.1002/qua.24757.
[53] Yanai T, Tew DP, Handy NC. A new hybrid exchange-correlation functional using the Coulomb-attenuating method (CAM-B3LYP). Chem Phys Lett 2004;393(1–3):51–7. https://doi.org/10.1016/j.cplett.2004.06.011.
[54] Truhlar DG, Garrett BC, Klippenstein SJ. Current status of transition-state theory. J Phys Chem 1996;100(31):12771–800. https://doi.org/10.1021/jp953748q.
[55] Konnov AA, Mohammad A, Kishore VR, Kim NI, Prathap C, Kumar S. A comprehensive review of measurements and data analysis of laminar burning velocities for various fuel plus air mixtures. Prog Energy Combust Sci 2018;68:197–267. https://doi.org/10.1016/j.pecs.2018.05.003.
[56] Ren F, Chu HQ, Xiang LK, Han WW, Gu MY. Effect of hydrogen addition on the laminar premixed combustion characteristics the main components of natural gas. J Energy Inst 2019;92(4):1178–90. https://doi.org/10.1016/j.joei.2018.05.011.
[57] Li P, Ke B, Zhang J, Chen XF. Numerical investigation of the chemical effect and inhibition effect improvement of $C_3H_2F_3Br$ (2-BTP) using the perfectly stirred reactor model. Energies 2018;11(10):1–11. https://doi.org/10.3390/en11102670.
[58] Yamamoto O, Takahashi K, Inomata T. Kinetic studies on the reactions of heptafluorpropanes with O ($^3$P) and H atoms at high temperatures. J Phys Chem A 2004;108(8):1417–27. https://doi.org/10.1021/jp036669k.
[59] Su B, Luo ZM, Wang T, Xie C, Cheng FM. Chemical kinetic behaviors at the chain initiation stage of $CH_4/H_2$/air mixture. J Hazard Mater 2021;403:123680. https://doi.org/10.1016/j.jhazmat.2020.123680.
[60] Gatsonides JG, Andrews GE, Phylaktou HN, Chattaway A. Fluorinated halon replacement agents in explosion inerting. J Loss Prev Process Ind 2015;36:544–52. https://doi.org/10.1016/j.jlp.2015.03.001.
[61] Cheng Y, Tang CL, Huang ZH. Kinetic analysis of $H_2$ addition effect on the laminar flame parameters of the C1–C4 n-alkane-air mixtures: From one step overall assumption to detailed reaction mechanism. Int J Hydrogen Energy 2015;40(1):703–18. https://doi.org/10.1016/j.ijhydene.2014.11.010.
[62] Babushok VI, Burgess DR, Hegetschweiler MJ, Linteris GT. Flame propagation in the mixtures of $O_2/N_2$ oxidizer with fluorinated propene refrigerants ($CH_2CFCF_3$, $CHFCHCF_3$, $CH_2CHCF_3$). Combust Sci Technol 2020;193(11):1949–72. https://doi.org/10.1080/00102202.2020.1720663.
[63] Needham CD, Westmoreland PR. Combustion and flammability chemistry for the refrigerant HFO-1234yf (2,3,3,3-tetrafluoropropene). Combust Flame 2017;184:176–85. https://doi.org/10.1016/j.combustflame.2017.06.004.